ELSEVIER

Catalysis Today 77 (2003) 371–384

CATALYSIS TODAY

www.elsevier.com/locate/cattod

Spectroscopic characterisation of microporous aluminophosphate materials with potential application in environmental catalysis

A. Frache [a], E. Gianotti [b], L. Marchese [a,*]

[a] *Dipartimento di Scienze e Tecnologie Avanzate, Università del Piemonte Orientale "A. Avogadro", C.so Borsalino 54, 15100 Alessandria, Italy*

[b] *Dipartimento di Chimica IFM, Università di Torino, Via P. Giuria 7, 10125 Torino, Italy*

Abstract

This review article deals with a spectroscopic characterisation, including FTIR, UV-Vis-NIR and NMR, of acid and redox microporous aluminophosphate catalysts with chabasite-related structure. These materials show high thermal and hydrothermal stability, and for this reason are attractive catalysts for environmental application. An extended investigation of acid SAPO-18 and SAPO-34, which are selective catalysts in methanol-to-olefins (MTO) and oxidative dehydrogenation (ODH) of light alkanes processes, will be presented. These catalysts can also be used as supports for the preparation of metal-containing molecular sieves for De-NO_x reactions. Catalytic studies of NO oxidation to NO_2 and N_2O decomposition performed on cobalt- and copper-containing materials will be illustrated and correlated to spectroscopic results.

Keywords: Aluminophosphate molecular sieves; Environmental catalysis; CO/NO adsorption; Spectroscopic characterization

1. Introduction

Aluminophosphate (AlPO-*n*) and silicoaluminophosphate (CO/NO adsorption; Spectroscopic characterisation) molecular sieves form a new class of microporous crystalline materials comparable to well-known zeolites. The structures of AlPOs and SAPOs molecular sieves cover a range of different structure types; some are analogous to certain zeolites such as SAPO-42 (structure similar to zeolite A) or SAPO-34 (chabasite structure), but a large number of AlPOs, such as AlPO-5 or VPI-5, have a unique structure with no zeolite analogue. The incorporation of transition metal ions into framework sites of the AlPOs and SAPOs molecular sieves is also of particular interest for the design of novel catalysts [1,2]. The location and structure of the reactive metal ion site is of considerable importance for understanding the chemistry of such materials [1].

Brønsted acid sites in zeolites can be formally represented as Si–O(H)–Al [3–5] and similar centres are present in microporous SAPOs [5–7]. The neutral framework of AlPOs is formed corner-sharing AlO_4 and PO_4 tetrahedral units, and the substitution of Si(IV) for some P(V) produces negatively charged oxygens which are balanced by protons (Scheme 1).

Brønsted acidity may be also produced in metal-aluminophosphates (MeAPOs) [1]. In fact, when divalent metal cations (Me: Co, Mg, Zn, Ni, etc.) substitute for trivalent aluminium, again protons which balance the negatively charged framework are needed. In this case, hydroxyls which are bridged between phosphorous and the divalent cations [8–11] are obtained (Scheme 1). However, when cobalt ions (or other transition metal ions including Ti^{4+}, V^{5+}, Cr^{3+},

* Corresponding author.
E-mail address: leonardo.marchese@unito.it (L. Marchese).

0920-5861/02/$ – see front matter
doi:10.1016/S0920-5861(02)00381-4

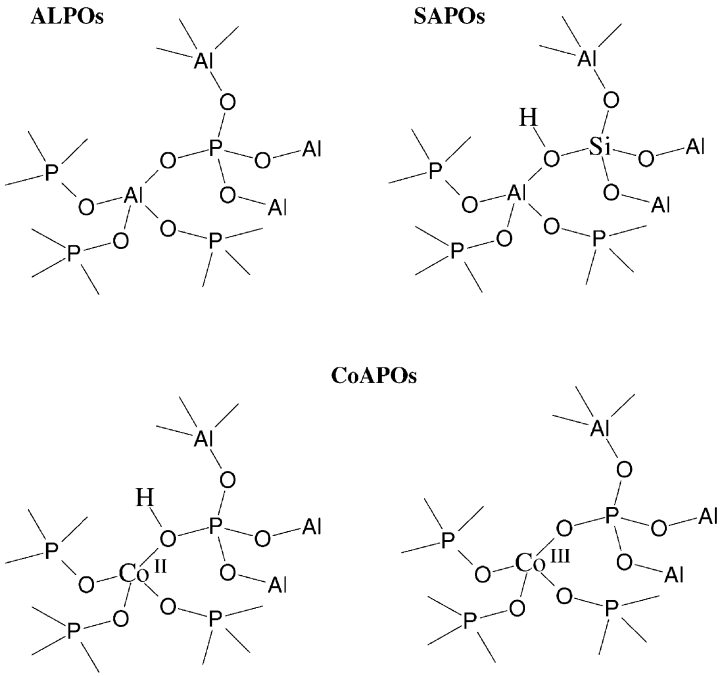

Scheme 1.

Mn^{2+}, etc.) are introduced into the AlPO framework, even more interesting redox molecular sieves are obtained [1,4,5].

A variety of spectroscopic techniques, including FTIR, UV-Vis-NIR, NMR and ESR, have been used, even with the aid of molecular probes, for monitoring the local structure of active centres in SAPOs and MeAPOs microporous catalysts. Though NO has been frequently used as molecular probe of transition metal ions in zeolites [12,13], studies of NO dissociation on metal ion-exchanged ZSM-5 have opened more attractive prospective. It was found, in fact, that Cu-ZSM-5 has high activity towards the decomposition of NO directly to N_2 and O_2 and this property was attributed to the presence of redox Cu^+/Cu^{2+} couples [14–16].

More recently, many efforts have also been focused on cobalt ion-exchanged zeolites (CoZSM-5, Co-mordenite, Co-Y, Co-X, Co-ferrierite) as they revealed an high activity in the selective catalytic reduction (SCR) of NO_x by ethene and methane in the presence of oxygen [17–22]. However, zeolite-based systems are of growing interest for their high performances under clean laboratory conditions, although their lack of stability under real operating conditions seems to be an unavoidable limitation [23–25].

In this context, some metal-containing AlPOs and SAPOs with redox properties have been found attractive for their resistance to the presence of water vapour [26,27], although they have not been extensively studied for $DeNO_x$ reactions. Good catalytic performances of Cu-SAPO-34 in SCR of NO with propene [28], Cu–Me-AlPO-11 (Me: Mg^{2+} and Zn^{2+}) in NO decomposition [29] and CoAPO-34 in NO oxidation to NO_2 [30] were reported.

Some selected examples of acid and redox AlPOs with high hydrothermal stability will be presented in this review article. Particular emphasis will be given to spectroscopic studies on catalysts with chabasite-related structure, such as Si-, Co-, Cu-containing AlPO-34 and Co-containing AlPO-18.

2. Synthesis and structural characterisation

The synthesis of AlPOs, SAPOs or MeAPOs molecular sieves typically uses an aqueous reaction mixture formed by an alumina source (e.g. pseudo-boehmite or

Table 1
Molar composition of gels used for the molecular sieve crystallisation[a]

Samples	Me	Al	P	Si	Morpholine	HF	H_2O
AlPO-34	–	1.00	1.00	–	1.25	0.35	50
SAPO-34	–	1.00	0.90	0.25	1.25	–	50
CuAPO-34	x	$1-x$	1.00	–	1.25	0.35	50
CuAPSO-34	x	$1-x$	0.90	0.25	1.25	–	50
CoAPO-34	x	$1-x$	1.00	–	1.25	0.35	50
CoAPSO-34	x	$1-x$	0.90	0.25	1.25	–	50

[a] Me: Co or Cu; x may vary from 0.04 to 0.2.

aluminium isopropoxide) and the diluted orthophosphoric acid, then the template, an amine or quaternary ammonium hydroxide, is added [31]. Amorphous SiO_2 is normally used as silica source for the synthesis of SAPO-34, and solutions of metal ions are used for MeAPOs. These gels are crystallised in autoclaves at temperatures between 353 and 473 K under autogenous pressure for times varying from few hours to several days.

Co-containing AlPOs were prepared by adding cobalt acetate at the synthesis gel whereas sample with copper by adding CuO to the orthophosphoric acid for a complete dissolution of the salt [32]. Table 1 shows some examples of gel composition used for the crystallisation.

Some of these samples showed an high thermal stability as found by in situ X-ray diffraction (XRD) at increasing temperatures. Fig. 1 shows the XRD patterns of SAPO-34, CuAPSO-34 and CoAPSO-34 recorded at 900 °C, and suggests that in all cases the chabasite structure was essentially retained at this temperature [33].

However, only the sample which did not contain transition metal ions, kept a nearly pure chabasite phase. Additionally, there were significant differences between the spectra of cobalt and copper-containing

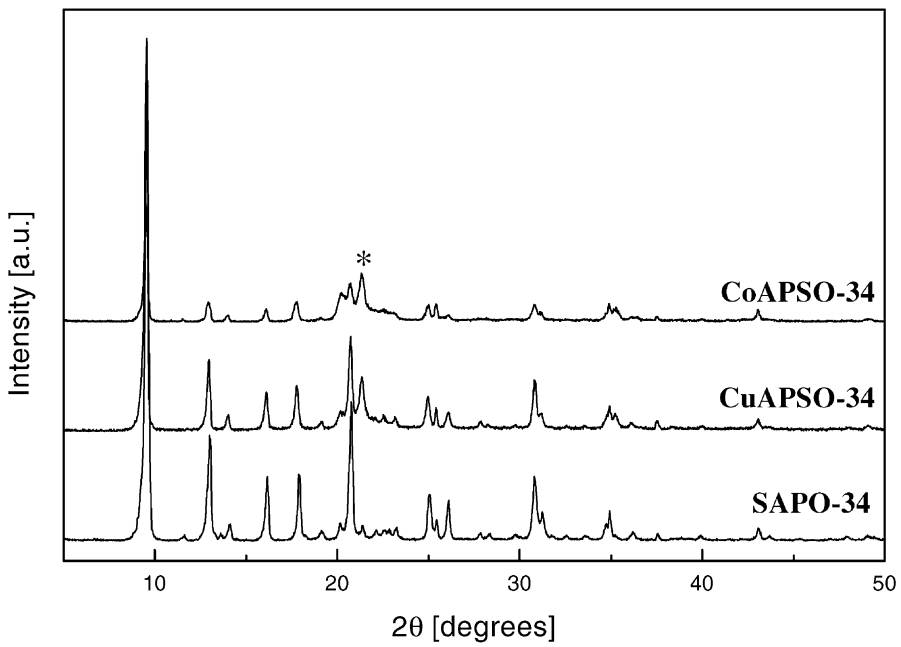

Fig. 1. XRD patterns of SAPO-34, CuAPSO-34 and CoAPSO-34 at 900 °C after template removal: (∗) reflection due to tridimite dense phase (reproduced from Ref. [34]).

MeAPSO-34 samples. In fact, CuAPSO-34 showed a behaviour similar to SAPO-34, indicating a high thermal resistance of the framework, only a small fraction of the material is transformed to tridimite dense phase (reflection at $2\theta = 21.3^\circ$ value). CoAPSO-34 instead, showed a higher loss of the initial crystallinity and the appearance of a higher fraction of tridimite phase. As a consequence, Cu-containing systems seem to be more stable than the corresponding Co-containing ones [34]. Noteworthy, these studies showed that CuAPSO-34 catalysts have also a high hydrothermal stability after mild steam ageing treatments [26,34] and this makes these materials very attractive for practical applications in environmental catalysis.

3. Spectroscopic characterisation

3.1. Host–guest interaction in SAPO-34

Molecular complexes or aggregates of templating molecules may play a decisive role in the formation of desired materials and remain embedded inside the inorganic network in the final product (Fig. 2).

A combination of FTIR and Raman spectroscopy was used to monitor the molecular interactions which occur within the chabasite cages of as-synthesised SAPO-34 where morpholine and water molecules are present. Evidences of the morpholine–framework (host–guest) and morpholine–morpholine and morpholine–water (guest–guest) interactions were reported [31]. Raman spectra of as-synthesised SAPO-34 is very similar to that of a solution of protonated morpholine obtained by addition of hydrochloric acid to pure morpholine and differ substantially from that of neutral morpholine [35]. This suggested that morpholine molecules in protonic form, $C_4H_8ONH_2^+$ (morpholinium), are entrapped inside the cages of SAPO-34. Evidences of the confinement of the protonated morpholine were obtained by comparing the Raman spectrum of the synthesis gel recorded before the crystallisation and the final, well-crystallised, SAPO-34 [31]. A very recent single crystal XRD and FTIR combined study showed that MH^+–H_2O–H_2O–MH^+ chains are embedded within the chabasite network of as-synthesised SAPO-34 (Fig. 2) [36].

3.2. Si-incorporation in chabasite-related SAPOs

SAPO-18 and SAPO-34 are acid catalysts for methanol-to-olefins (MTO) [37] and oxidative dehydrogenation (ODH) [38] processes. The incorporation

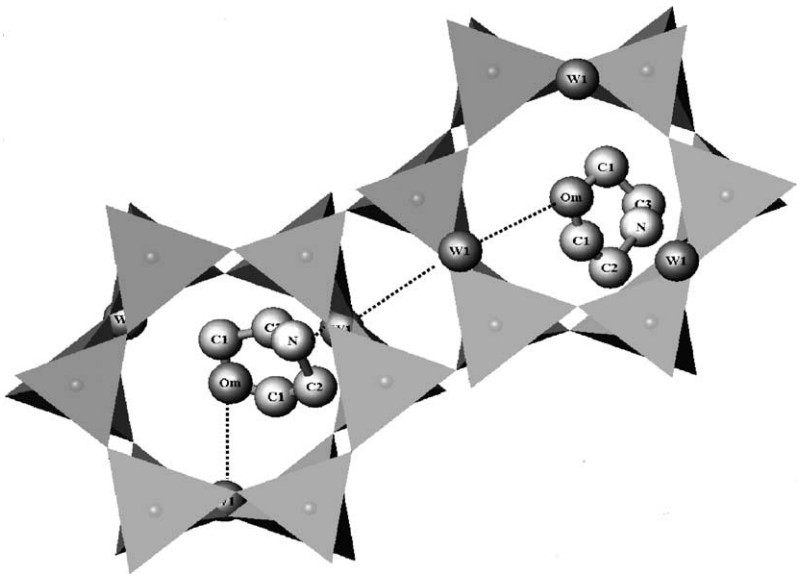

Fig. 2. Morpholinium (or morpholine)–water molecular complexes localised in a adjacent chabasite cages connected each other by hydrogen bonds to symmetrically equivalent water molecules at the W1 sites to form MH^+–H_2O–H_2O–MH^+ (or MH^+–H_2O–H_2O–M) chains.

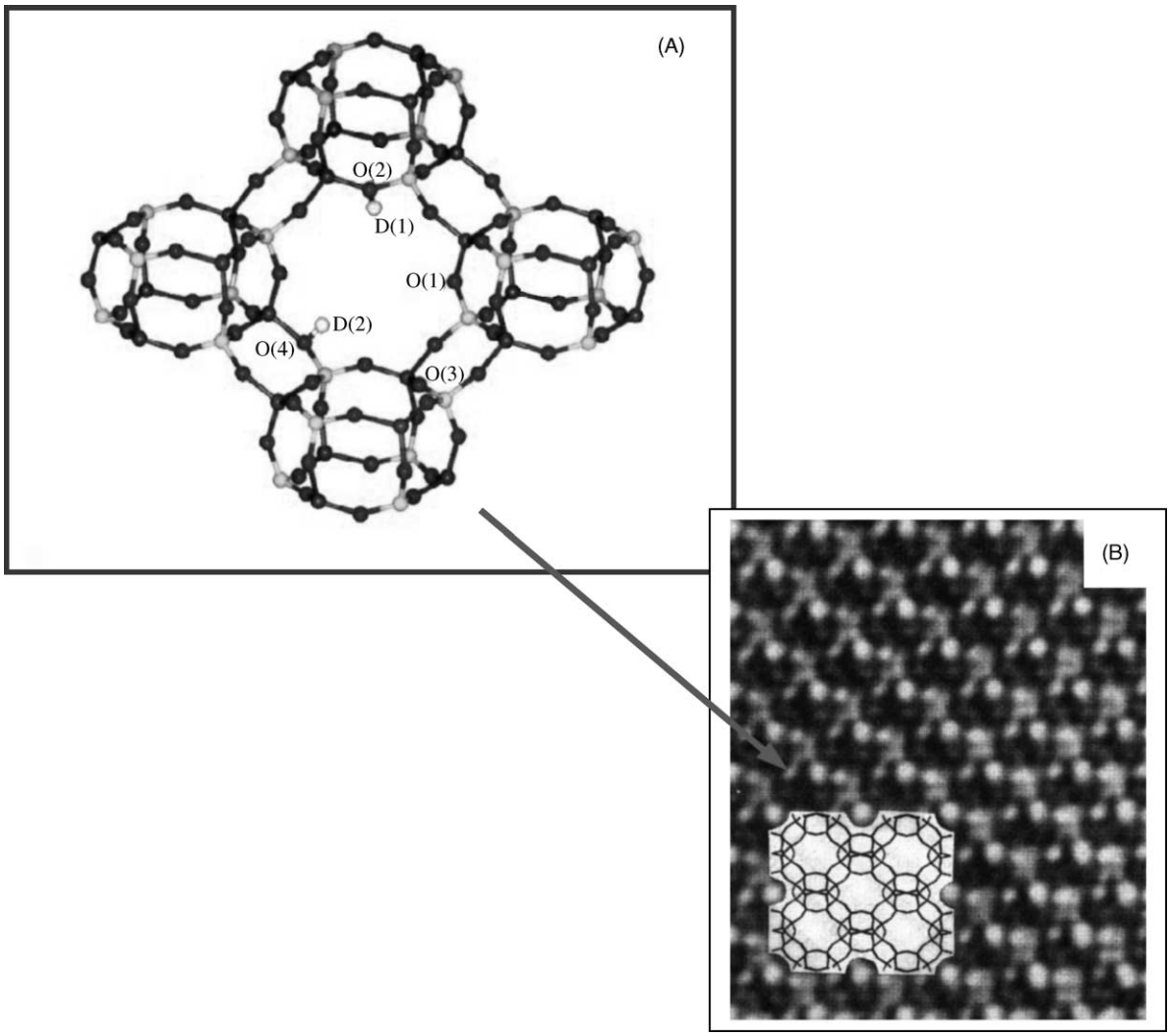

Fig. 3. (A) A ball and stick representation of the structure of dehydrated HSAPO-34; (B) HRTEM image of SAPO-18 taken down to the [0 0 1] direction (adapted from Refs. [7,39]).

of silicon via direct synthesis into AlPO-18 (AEI structure code), which has a framework structure related to, but crystallographically distinct from, that of the well-known solid acid catalyst SAPO-34 (CHA structure code) (Fig. 3), was investigated by a range of techniques.

^{29}Si MAS NMR spectroscopy revealed that silicon substitutes for both phosphorous and aluminium in SAPO-18, whereas in SAPO-34, substitutes only for phosphorous and leads to a larger number of Brønsted acid sites. Infrared and ^{1}H MAS NMR spectroscopies and TPD of ammonia were used to examine the Brønsted acid sites in SAPO-18 samples [38].

The different silicon-substitution mechanism for SAPO-18 and SAPO-34 was confirmed by FTIR spectroscopy. The infrared spectra of template-free AlPO-18 and SAPO-18 samples within the hydroxyl stretching absorption region are shown in Fig. 4A.

AlPO-18 has one main absorption band at 3676 cm^{-1}, attributable to P–OH groups and these were observed for almost all AlPO-based molecular sieves. For AlPO-18, besides the main P–OH

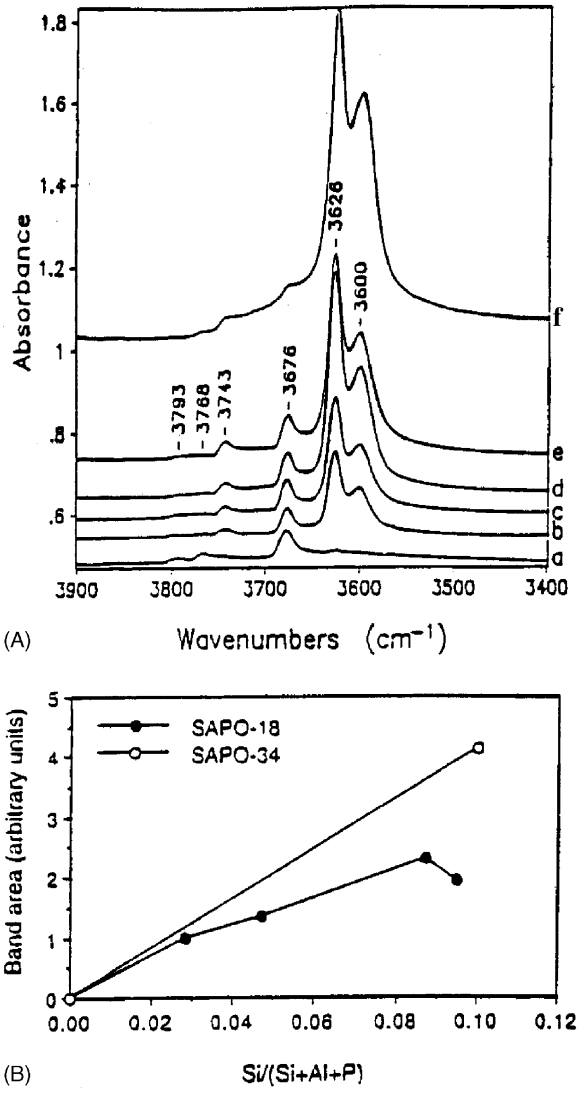

Fig. 4. (A) Infrared spectra of: (a) AlPO-18; (b)–(e) SAPO-18 with different amount of silicon; (f) SAPO-34. (B) Peaks at 3626 and 3600 cm^{-1} are those attributed to bridging hydroxyls versus framework $Si/(Si + Al + P)$ for the SAPO-34 and the SAPO-18 samples (reproduced from Ref. [39]).

absorption, there are two bands at 3768 and 3793 cm^{-1}, attributed to Al–OH groups. In addition to the P–OH and Al–OH absorption observed for AlPO-18, template-free SAPO-18 samples possess two other distinct absorption peaks at 3600 and 3626 cm^{-1} due to bridging OH groups and one less intense band at 3743 cm^{-1}. The 3743 cm^{-1} band was

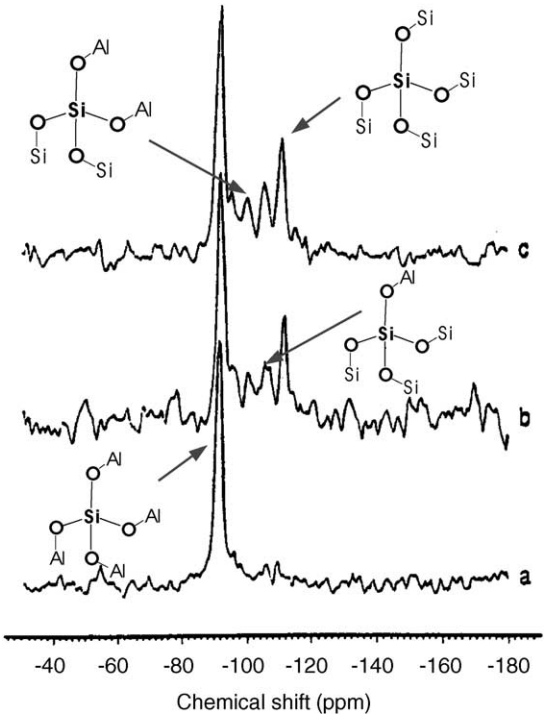

Fig. 5. ^{29}Si NMR spectra for as-synthesised: (a) SAPO-34 (with $Si/(Si + Al + P) = 0.1$); (b) SAPO-18 (with $Si/(Si + Al + P) = 0.047$); (c) SAPO-18 with $Si/(Si + Al + P) = 0.087$) (adapted from Ref. [40]).

assigned to Si–OH groups. The 3600 and 3626 cm^{-1} peaks were first observed for SAPO-34 [40,41]. In the case of SAPO-18, the overall intensity of the two bridging hydroxyl peaks (as calculated from their areas) increased with the amount of silicon in the structure (Fig. 4B). SAPO-34 showed a much higher concentration of bridging OH groups than all of the SAPO-18 samples.

Fig. 5 shows ^{29}Si MAS NMR spectra of two samples of the SAPO-18 with different Si amount in comparison with a SAPO-34 with $Si/(Si + Al + P) = 0.1$. SAPO-34 exhibited a single resonance at a chemical shift of −92 ppm, and this resonance was assigned to silicon surrounded by four AlO_4 neighbours.

The two similar SAPO-18 spectra each possessed two well-defined signals at −92 and −111 ppm, respectively, as well as three less intense peaks between them at chemical shifts of −96, −100, and −105 ppm, respectively. The first signal was again attributed to isolated silicon atoms substituting for phosphorous.

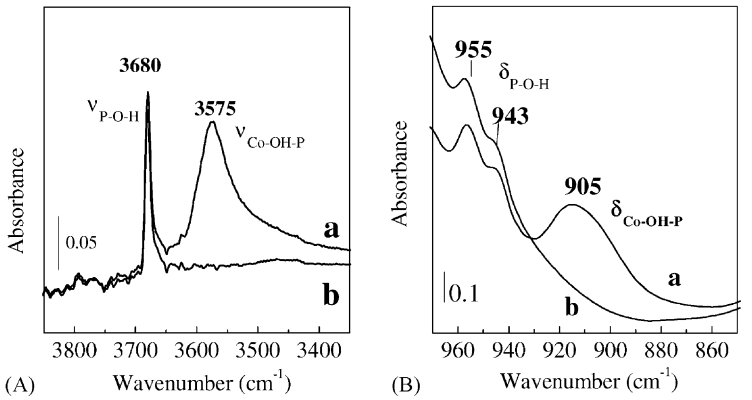

Fig. 6. FTIR spectra CoAPO-18 catalyst after reduction in H_2 at 673 K (curve a) and after calcination in O_2 at 823 K (curve b).

The other peaks were assigned to silicon surrounded by ($3AlO_4$ and $1SiO_4$), ($2AlO_4$ and $2SiO_4$), ($1AlO_4$ and $3SiO_4$), and ($4SiO_4$), respectively, in a fashion similar to that for aluminosilicate zeolites [42].

Altogether these results confirmed that silica islands are present in SAPO-18 catalysts and that the chabasite-type framework of SAPO-34 is able to incorporate more isolated Si ions responsible of the presence of Brønsted acid sites.

3.3. CoAPO-18: an acid and redox catalyst

The surface properties of CoAPO-18 catalysts have been studied by several spectroscopies tools, including FTIR, diffuse reflectance UV-Vis and X-ray absorption spectroscopy (XAS) [43]. FTIR spectra (Fig. 6) revealed that the reduced template-free catalyst (curve a) has bands at 3575 cm^{-1} and 905 cm^{-1} which were assigned, respectively, to stretching and in-plane bending vibrations of hydroxyl groups bridging between Co^{2+} and P (ν_{OH} and δ_{OH}).

It was therefore proved that Co^{2+} substituted isomorphously for Al^{3+} in the lattice of the AlPO-18 structure, and this was also confirmed by UV-Vis and EXAFS measurements. After calcination in O_2 at 823 K (curve b) only peaks at 3680 and 955 cm^{-1} assigned to the stretching vibration of P–OH groups in lattice defects (internal and external surface defects) were present [11]. A very small absorption at 943 cm^{-1} was present both in calcined and reduced CoAPO-18 which was not found in AlPO-18. This band was related to the presence of Co^{2+} Lewis acid sites [11].

To have a better understanding of the catalytic behaviour of CoAPO-18, it was important to define in quantitative terms the environment of the cobalt ion in the calcined and reduced states. This was achieved from a series of in situ measurements at increasing temperatures using synchrotron radiation and recording simultaneously EXAFS spectra and XRD patterns. From 50 to 625 °C, there were no significant changes in the diffraction patterns demonstrating that the framework remained intact through the burn-out of the template and the subsequent activation of the catalyst. The shift in the cobalt K-edge of 1.2 eV, an increase in the pre-edge feature at 7710 eV and a decrease in frequency of the EXAFS oscillations proved that during the calcinations Co^{2+} ions were oxidised to Co^{3+} [44].

DR UV-Vis-NIR and FTIR spectroscopic studies, supplemented by the use of probe molecules as selective adsorbates (N_2 [9,10], CO [9,30], C_2H_4 [9] and H_2O [11]), clarified the atomic environment of cobalt centres in CoAPO-18 solid acid catalysts. The DR UV-Vis-NIR spectra of the as-synthesised CoAPO-18 material (Fig. 7, curve a) have absorptions (triplet bands) in the visible (20,000–15,000 cm^{-1}) and in the near infrared (10,000–4000 cm^{-1}) regions attributable to $^4T_1(P) \leftarrow {}^4A_2(F)$ and $^4T_1(F) \leftarrow {}^4A_2(F)$ ligand field transitions of tetrahedrally coordinated Co^{2+}, from which fact the substitution of cobalt(II) ions for Al in framework positions was inferred. After

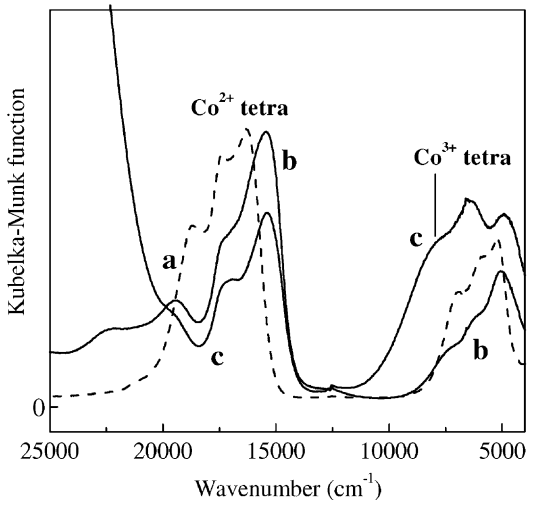

Fig. 7. Diffuse reflectance UV-Vis-NIR spectra of as-synthesised CoAPO-18 (curve a), after reduction (curve b) and after calcination (curve c) (adapted from Ref. [9]).

reduction in H_2 at 400 °C (Fig. 7, curve b), Co^{2+} ions resulted in more distorted tetrahedral environments and a fraction was also present as Lewis acid centres [9,11]; only a portion (nearly 50%) of tetrahedral Co^{2+}, in fact, generated Brønsted acid sites (bridged OH).

Structural Co^{2+} ions, those associated with bridged OH, could be oxidised to structural Co^{3+} ions (with tetrahedral coordination) and contemporaneously protons eliminated (Fig. 6, curve b). After calcination in O_2 at 550 °C (Fig. 7, curve c), nearly 50% of cobalt was still divalent and did not generate protons (Fig. 6, curve b); they could either be in tetrahedral coordination or in coordinatively unsaturated Lewis centres [9].

Moreover, a broad adsorption at 9000–8000 cm^{-1} was present (Fig. 7, curve c) and assigned to $^5T_2 \rightarrow {}^5E$ transition of tetrahedral Co^{3+} ions in structural $[CoO_4]$ units [45,46]. Co^{2+}/Co^{3+} redox couples were also found in CoAPO-34 catalyst [30].

EPR studies performed at 77 K showed that cobalt ions in high spin state are present in framework positions both in CoAPO-18 and CoAPO-34 systems.

Both the as-prepared samples (which contain the organic template), the reduced and the calcined samples exhibited a broad, asymmetric and unresolved spectrum typical of d^7 high spin Co^{2+} ions. The intensity of the spectrum after oxidation of the template was lower than that of the as-prepared material due to a partial oxidation of Co^{2+} ions to Co^{3+} (EPR silent) [47].

4. MeAPO-34 materials with potential application in environmental catalysis

The bifunctional, redox and acid, behaviour of MeAPOs and MeAPSOs (Me: Co and Cu) systems was investigated by CO and NO adsorption using FTIR spectroscopy [30,32,34,48] and some of these results will be summarised in the following sections. Some correlations between spectroscopic and catalytic results will be also enlightened.

4.1. CoAPO-34

CO adsorption at 298 K on CoAPO-18 (Fig. 8A) and CoAPO-34 (Fig. 8B) materials in connection with the OH evolution evidenced that only tetrahedral Co^{2+} ions can be oxidised to Co^{3+} ions under thermal treatments [9,30].

CO molecules linearly adsorbed on Co^{2+} ions, mainly located in framework positions, were evidenced both in CoAPO-18 and CoAPO-34 catalysts by the presence of two absorptions at 2180 and 2185 cm^{-1}. The band at 2180 cm^{-1} was assigned to Co^{2+} ions in tetrahedral coordination, those related to Brønsted acid sites, whereas the absorption at 2185 cm^{-1} was assigned to tricoordinated Co^{2+} Lewis acid sites in framework defects. After calcination in O_2 at 550 °C, only the band at 2180 cm^{-1} decreased in intensity, and a new absorption at 2178 cm^{-1} was observed only for CoAPO-34. The decrease in intensity of the band at 2180 cm^{-1} after oxidation was associated to the fact that only the Co^{2+} ions related to Brønsted acid sites could be oxidised to Co^{3+} ions.

The CO adsorption at 298 K on CoAPO-34 catalysts with different Co loading allowed to calculate the fraction of Co^{2+} ions which could be oxidised to Co^{3+} under thermal treatments. Three CoAPO-34 catalysts with different cobalt loading ($Co/(Co + Al) = 0.04$, 0.08 and 0.2 in the synthesis gel) were studied [30]. The concentration of oxidisable Co^{2+} ions (reported in Table 2) was determined by using the Beer's law, $A = \varepsilon N \rho$, where A is the intensity of the band of

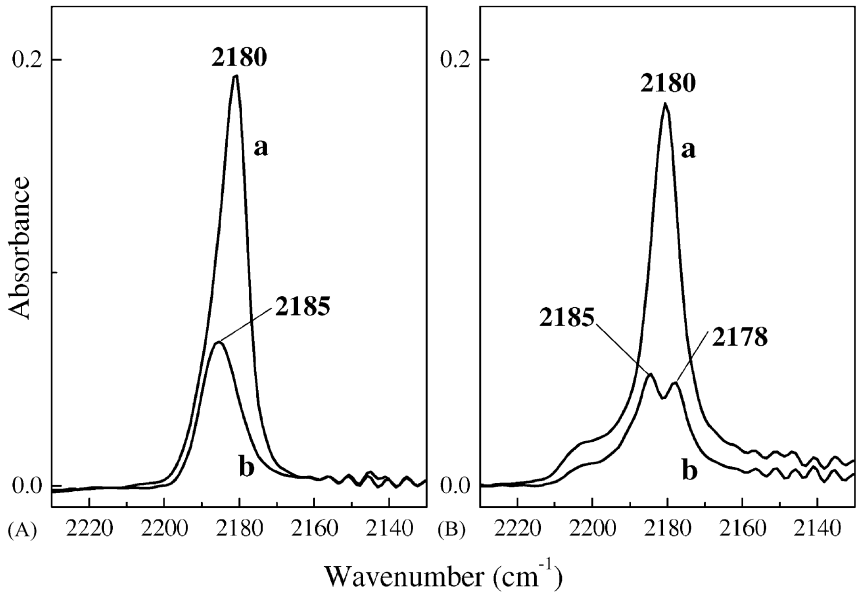

Fig. 8. FTIR spectra of CO adsorbed at 298 K on CoAPO-18 (A) and CoAPO-34 (B). Curve a: reduced samples, curve b: oxidised samples.

adsorbed CO (cm^{-1}), ε the integrated extinction coefficient ($cm\,\mu mol^{-1}$), N the concentration of the adsorbed CO ($mmol\,g^{-1}$) and ρ the density of the pellet ($mg\,cm^{-2}$) used for the FTIR analysis. The value of $\varepsilon = 1.0$ reported for CO adsorbed on cobalt exchanged zeolite Y [49] was used and the CO:Co^{2+} = 1:1 stoichiometry assumed.

NO adsorption at 298 K (Fig. 9) on reduced (curves a and c) and oxidised (curves b and d) CoAPO-18 and CoAPO-34 catalysts produced, though of different amount, dinitrosyl complexes on Co^{2+} ions (bands in the range of 1950–1750 cm^{-1}).

It was possible to distinguish two family of dinitrosyls: bands at 1910 and 1838 cm^{-1} due to NO groups adsorbed on Co^{2+} sites in framework positions associated with Brønsted acid sites (Scheme 2, structure A), and bands at 1898 and 1814 cm^{-1} attributed to dinitrosyl species on Co^{2+} Lewis acid sites (Scheme 2, structure B) [43,47,48].

The intensity of the dinitrosylic bands was lower in oxidised samples (curves b and d) respect to those observed in reduced samples (curves a and c), because following this thermal treatment a fraction of Co^{2+} ions was oxidised to Co^{3+} ions. Moreover, a band at 2160 cm^{-1} in the case of CoAPO-18 and at 2151 cm^{-1} in of CoAPO-34 were also formed and were particularly evident in the oxidised samples. This band was assigned to NO_2-like complexes for an absorption in

Table 2
Cobalt ions concentration used for the gel crystallisation and measured by CO adsorption on CoAPO-34 catalysts using FTIR spectroscopy

	Cobalt concentration (mmol Co/g_{cat})[a]	Adsorbed CO (cm^{-1}/mg cm^{-2})[b]		Concentration of oxidable Co^{2+} (mmol Co/g_{cat})[c]
		Oxidised	Reduced	
CoAPO-34 (4)	0.32	0.16	0.37	0.21
CoAPO-34 (8)	0.65	0.36	0.73	0.37
CoAPO-34 (20)	1.56	0.24	0.40	0.16

[a] Cobalt concentration used in the synthesis gel.
[b] Integrated area (cm^{-1}) normalised respect to the density of the pellets ($mg\,cm^{-2}$).
[c] Determined by assuming $\varepsilon = 1.0\,cm\,\mu mol^{-1}$ [46].

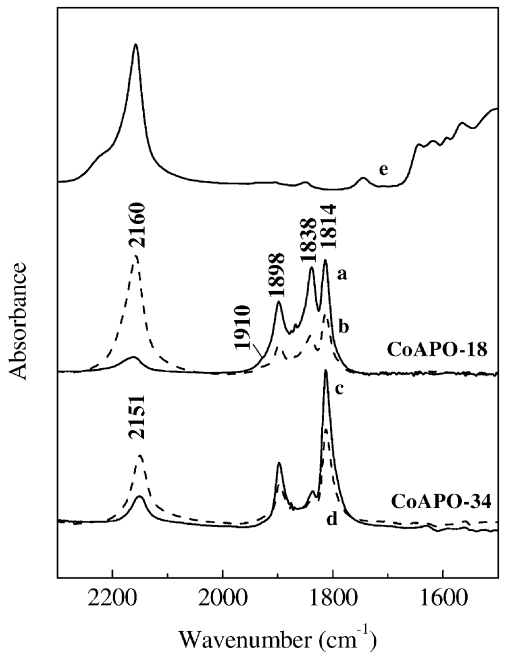

Fig. 9. FTIR spectra of NO adsorbed at 298 K on CoAPO-18 and CoAPO-34. Curves a and c: reduced samples; curves b and d: oxidised samples; curve e: FTIR spectrum of NO_2 adsorbed at 298 K on reduced CoAPO-18.

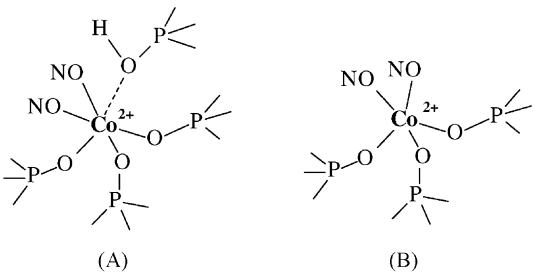

Scheme 2.

this position was found upon NO_2 adsorption at 298 K on Co^{2+} ions (Fig. 9, curve e). The mechanism of formation of such complexes and their nature was not clarified, however it was proposed that NO may interact both with Co^{3+} ions and framework oxygen forming a NO_2-like species (Scheme 3) [47–50].

On the reduced samples, the NO_2 complexes were formed slowly and the related bands less intense; this behaviour suggested that NO can oxidise a fraction of Co^{2+} ions to Co^{3+} and this was confirmed by the DR UV-Vis-NIR spectra (not reported) [43,48]. The interaction of NO with these newly formed Co^{3+} sites is represented in Scheme 3.

4.2. Catalytic tests

The redox behaviour of CoAPO-34 catalysts was first evaluated in the NO oxidation to NO_2 and the results are summarised in Fig. 10.

The AlPO-34 Co-unloaded sample was not active at all in the experimental conditions investigated, whereas CoAPO-34 reduced sample showed a very high and stable activity (on 24 h run-time observation). The NO conversion reached the equilibrium value at 350 °C, a similar behaviour was observed for Cu-ZSM-5 zeolite, the most active catalyst in both NO decomposition and NO reduction with hydrocarbons [51]. On the contrary, the oxidised CoAPO-34 showed a much lower activity, only above 450 °C, in fact, a very low NO conversion was observed. This result strongly supported the fact that only Co^{2+} centres are the active sites in NO oxidation.

The comparison between the catalytic activity of reduced CoAPO-34 (0.04), CoAPO-34 (0.08) and CoAPO-34 (0.2) in the NO oxidation to NO_2 is reported in Fig. 10B. It was found that CoAPO-34

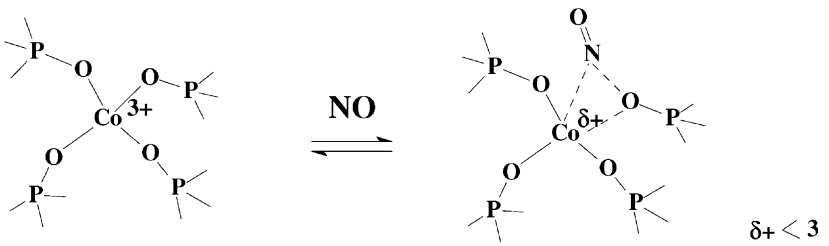

Scheme 3.

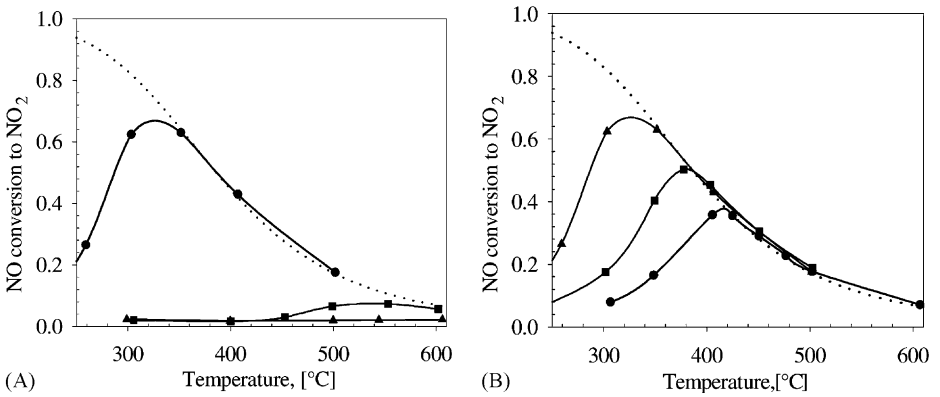

Fig. 10. (A) NO conversion to NO_2 on both reduced (●) and oxidised (■) CoAPO-34 catalyst compared to AlPO-34 (▲). Dotted line represents the equilibrium conversion. (B) NO conversion to NO_2 on reduced CoAPO-34 catalysts with different cobalt loading. (π) Co/(Co + Al) = 0.08; ($'$) Co/(Co + Al) = 0.04; ( ) Co/(Co + Al) = 0.2 (adapted from Refs. [30,43]).

(0.08) was the most active catalyst whereas the lowest activity among the three samples was exhibited by CoAPO-34 (0.2). The catalytic activity correlated very well with the concentration of Co^{2+}/Co^{3+} redox sites (the concentration of oxidisable sites reported in Table 2) determined by CO adsorption.

The activity of these catalysts in more interesting SCR reactions of NO with HC or CO [17,18,21,22] was also proved [52] and they revealed lower performances when compared to other Co-containing systems.

4.3. CuAPSO-34

4.3.1. CO adsorption

FTIR spectra of CO adsorbed on CuAPSO-34 (Fig. 11) suggested that $Cu^+(CO)_2$ dicarbonyl species formed at higher CO dosages (two sharp bands at 2175 and 2147 cm^{-1}, solid line) and that the dicarbonyls transformed into monocarbonyl $Cu^+(CO)$ complexes at lower CO dosages (one sharp band at 2152 cm^{-1}, dash line). Similar spectra were obtained for Cu-ZSM-5 [52–54].

This result evidenced the presence of Cu(I) species probably in the extra-framework positions of chabasite structure and these species are active in the $DeNO_x$ processes [28,29].

4.3.2. NO adsorption

The NO adsorption on CuAPSO-34 (Fig. 12) led to mono-nitrosyls on Cu^+ which absorb at 1805 cm^{-1}, whose intensity decreased slightly upon increasing NO pressure (curves 1–5) [48,51,53]. Mono-nitrosyls adsorbed on different Cu^{2+} sites in the region 1850–1950 cm^{-1} were also found, and their band intensities increased upon increasing NO dosages. Similar absorptions were reported for Cu-ZSM-5 and Cu-Y catalysts [17,55–57].

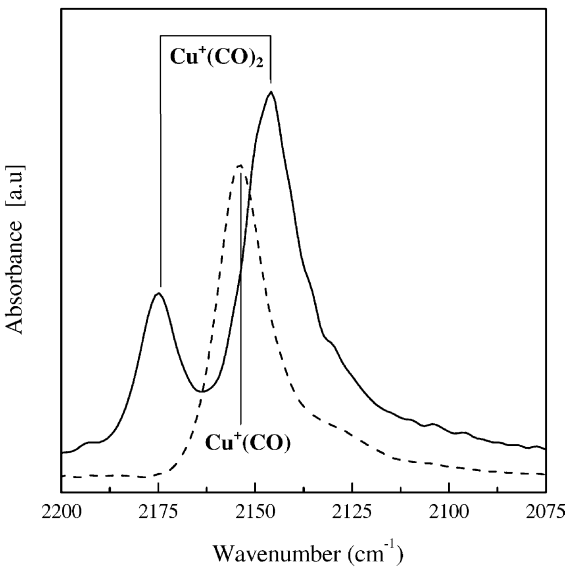

Fig. 11. FTIR spectra of CO adsorbed at 298 K on CuAPSO-34 (100 Torr CO, solid line; after evacuation at RT for 20 min, dashed line) (adapted from Ref. [34]).

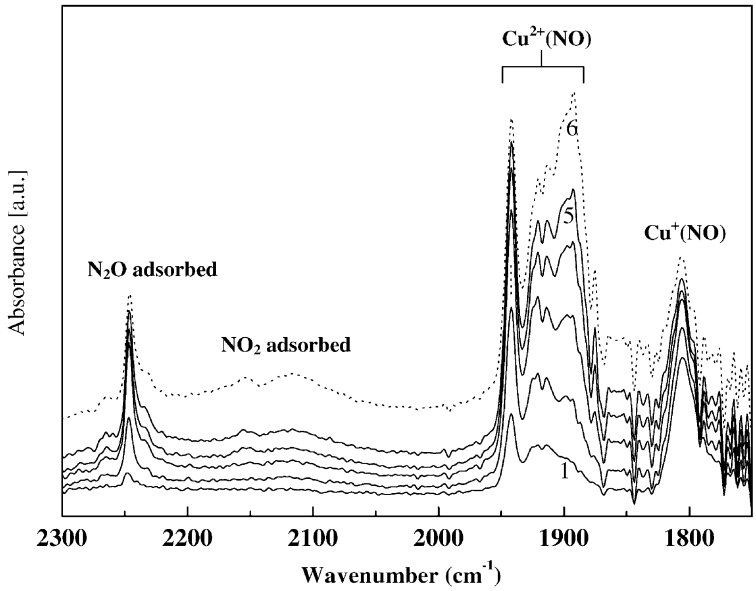

Fig. 12. FTIR spectra of NO adsorbed at 298 K on CuAPSO-34. Spectra 1–5 were recorded after increasing gradually the pressure from 0.5 to 50 Torr. Spectrum 6 (dotted line) was recorded after 30 min of contact with 50 Torr of NO (adapted from Ref. [34]).

Moreover, spectra recorded upon prolonged time of contact with higher NO dosages (curves 5 and 6) confirmed that a fraction of Cu^{+} ions could be transformed into Cu^{2+}, as generally found on Cu-ZSM-5. This redox behaviour has been frequently correlated to the catalytic properties of Cu-ZSM-5 in both NO and N_2O decomposition reactions [58,59]. Other bands which depended on both NO pressure and time of contact, were found. Bands in the region 2200–2100 cm^{-1}, due to linearly adsorbed NO_2 species [56], increased constantly whereas the band at 2244 cm^{-1}, due to adsorbed N_2O, increased with NO doses (Fig. 12, curves 1–5) and decreased with prolonged time of contact (Fig. 12, curves 5 and 6). This behaviour supported the proposal that both these species are intermediates of the NO decomposition to N_2 and O_2 [15,56] which was found to be active even on these catalysts.

4.3.3. Catalytic tests

N_2O decomposition both in the presence and in the absence of O_2 and water vapour in the feed was performed on copper-containing SAPO-34 and AlPO-34, with the aim of investigating not only activity properties of the different systems but also the stability of the catalysts. Fig. 13 shows the results of such tests carried out on CuAPSO-34, CuAPO-34 and Cu-ZSM-5 samples with a similar copper-loading. Cu-ZSM-5 was used as reference catalyst being, *under dry conditions*, the most active catalysts for N_2O decomposition (closed symbols). CuAPSO-34 also exhibited good activity in the range of temperatures from 400 to 600 °C, even in excess of oxygen (1 vol.%, as compared with N_2O feed content of 600 ppm), which resulted in a very weak depressing effect on N_2O conversion (dotted line).

CuAPO-34 catalyst is much less active than both Cu-ZSM-5 and CuAPSO-34, even though its copper content is nearly twice the one of the two other catalysts. This behaviour was in agreement with the spectroscopic results which showed that the number of Cu^{+} catalytic sites is less abundant in CuAPO-34. Although CuAPSO-34 has a lower catalytic activity than Cu-ZSM-5, its activity level is sustained after a long treatment (80 h) at 600 °C in the presence of H_2O (Fig. 13). On the contrary, Cu-ZSM-5 was unable to withstand an even milder treatment (60 h at 550 °C), as a nearly complete loss of catalytic activity was observed. However, this very low hydrothermal resistance of Cu-ZSM-5 was already known and represents the main limitation to its application [34].

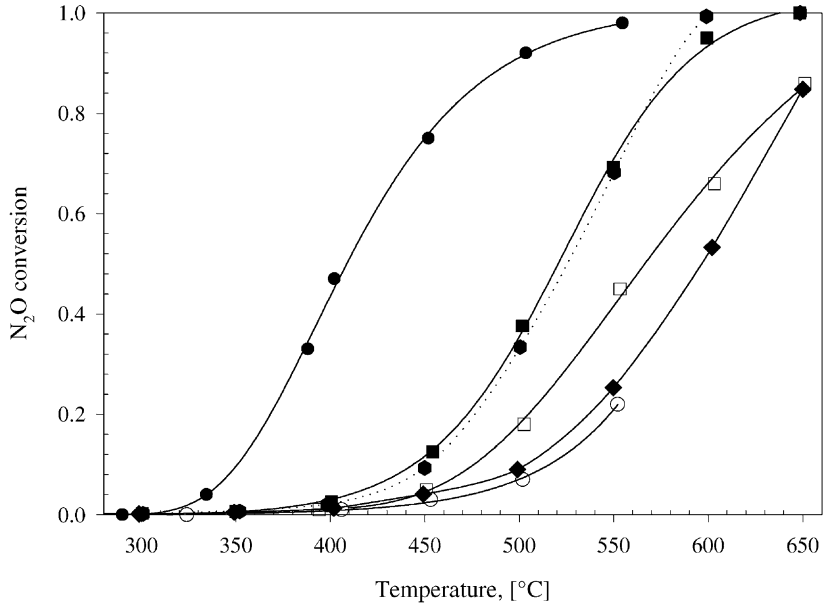

Fig. 13. N_2O conversion as a function of temperature over Cu-ZSM-5 (● and ○), CuAPSO-34(1.23) (■, ⬢ and □) and CuAPO-34 (◆). Feed: N_2O (600 ppm), O_2 (1% in vol.) only for (⬢) and balance He. $W/F = 0.1\,g\,s\,N\,cm^{-3}$. Open symbols represent catalytic test after ageing treatment (reproduced from Ref. [34]).

5. Conclusions

A multi-technique approach has been described to understand structure and morphology of catalysts and coordination and redox-state of the catalytic sites. The use of a variety of spectroscopic techniques, including FTIR, UV-Vis-NIR and NMR, has been shown for the characterisation of AlPOs, SAPOs and metal-containing MeAPOs and MeAPSOs microporous materials with chabasite-type structure.

Brønsted acid sites [Si–O(H)–Al] are present in SAPOs materials in that the isomorphous substitution of Si(IV) for some P(V) ions in the neutral AlPOs framework produces negatively charged oxygens which are balanced by protons. Brønsted acidity may be also present in MeAlPOs when divalent metal cations (Me: Mg^{2+}, Co^{2+}, Cu^{2+}, etc.) substitute for Al(III). Hydroxyls bridged between phosphorous and divalent cations [Me–O(H)–P] are formed in this case. These protons are exchangeable sites for the introduction of redox centres, such as Co^{2+}/Co^{+}, Cu^{2+}/Cu^{+}, etc., which leads to active catalysts for $DeNO_x$ reactions. However, when transition metal ions are introduced directly into the synthesis gel leading to the zeolite crystallisation, even more stable redox molecular sieves may be obtained and this is a necessary requirement when $DeNO_x$ reactions are run in the presence of H_2O and/or at high temperatures.

Acknowledgements

Funding by MURST (“Progetti di Rilevante Interesse Nazionale, Cofinanziamento 2000”) and the “Consorzio Interuniversitario di Chimica per l’Ambiente” (INCA) are gratefully acknowledged.

References

[1] M. Hartmann, L. Kevan, Chem. Rev. 99 (1999) 635.
[2] J.M. Thomas, Angew. Chem. Int. Ed. Engl. 38 (1999) 3589.
[3] J.M. Thomas, Faraday Discuss. 105 (1996) 1.
[4] A. Corma, Chem. Rev. 97 (1997) 2373.
[5] S. Coluccia, L. Marchese, G. Martra, Micropor. Mesopor. Mater. 30 (1999) 43.
[6] B. Zibrowius, E. Loffler, M. Hunger, Zeolites 12 (1992) 167.
[7] L. Smith, A.K. Cheetham, L. Marchese, E. Gianotti, J.M. Thomas, P.A. Wright, J. Chen, Catal. Lett. 41 (1996) 13.

[8] J. Chen, J.M. Thomas, J. Chem. Soc., Chem. Commun. 5 (1994) 603.
[9] L. Marchese, G. Martra, N. Damilano, S. Coluccia, J.M. Thomas, Stud. Surf. Sci. Catal. 101 (1996) 861.
[10] L. Marchese, E. Gianotti, N. Damilano, S. Coluccia, J.M. Thomas, Catal. Lett. 37 (1996) 107.
[11] L. Marchese, J. Chen, J.M. Thomas, S. Coluccia, A. Zecchina, J. Phys. Chem. 98 (1994) 13350.
[12] K.A. Windhorst, J.H. Lunsford, J. Am. Chem. Soc., Faraday Trans. 97 (1975) 1407.
[13] T. Izuka, J.H. Lunsford, J. Mol. Catal. 8 (1980) 391.
[14] W.-X. Zhang, H. Yahiro, N. Mizuno, J. Izumi, M. Iwamoto, Chem. Lett. (1992) 851.
[15] E. Giamello, D. Murphy, G. Magnacca, C. Morterra, Y. Shiona, T. Namura, M. Anpo, J. Catal. 136 (1992) 510.
[16] M. Iwamoto, H. Yahiro, N. Mizuno, W.-X. Zhang, Y. Mine, H. Furukawa, S. Kagawa, J. Phys. Chem. 96 (1992) 9360.
[17] Y. Li, J.N. Armor, J. Catal. 150 (1994) 376.
[18] Y. Li, T.L. Slager, J.N. Armor, J. Catal. 150 (1994) 388.
[19] B.J. Adelman, T. Beutel, G.D. Lei, W.H.M. Sachtler, J. Catal. 158 (1996) 327.
[20] K.A. Windhorst, J.H. Lunsford, J. Am. Chem. Soc., Faraday Trans. 97 (1975) 1407.
[21] W.X. Zhang, H. Yahiro, M. Iwamoto, J. Chem. Soc., Faraday Trans. 91 (1995) 767.
[22] D.B. Lukyanov, E.A. Lombardo, G.A. Sill, J.L. d'Itri, W.K. Hall, J. Catal. 163 (1996) 447.
[23] V.I. Pârvulescu, P. Grange, B. Delmon, Catal. Today 46 (1998) 233.
[24] J.N. Armor, Micropor. Mesopor. Mater. 22 (1998) 451.
[25] Y. Traa, B. Burger, J. Weitkamp, Micropor. Mesopor. Mater. 30 (1999) 3.
[26] A. Frache, B.I. Palella, M. Cadoni, R. Pirone, H.O. Pastore, L. Marchese, Top. Catal. 22 (2003) 53.
[27] M. Briend, R. Vomscheid, M.J. Peltre, P.P. Man, D. Barthomeuf, J. Phys. Chem. 99 (1995) 8270.
[28] T. Ishihara, M. Kagawa, F. Hadama, Y. Takita, J. Catal. 169 (1997) 93.
[29] J. Dedecek, J. Cejka, B. Wichterlová, Appl. Catal. B 15 (1998) 233.
[30] L. Marchese, E. Gianotti, G. Martra, S. Coluccia, B. Palella, R. Pirone, P. Ciambelli, Stud. Surf. Sci. Catal. C 130 (2000) 3005.
[31] L. Marchese, A. Frache, E. Gianotti, G. Martra, M. Causà, S. Coluccia, Micropor. Mesopor. Mater. 30 (1999) 145.
[32] A. Frache, L. Marchese, M. Cadoni, S. Coluccia, B. Palella, R. Pirone, P. Ciambelli, Stud. Surf. Sci. Catal. 140 (2001) 269.
[33] Y. Watanabe, A. Koiwai, H. Takeuchi, S. Hyodo, S. Noda, J. Catal. 143 (1993) 430.
[34] A. Frache, B. Palella, M. Cadoni, R. Pirone, P. Ciambelli, H.O. Pastore, L. Marchese, Catal. Today 75 (2002) 359.
[35] S. Ashtekar, P.J. Barrie, M. Hargreaves, L.F. Gladden, Angew. Chem. Int. Ed. Engl. 36 (1997) 876.
[36] A. Martucci, A. Alberti, G. Cruciani, A. Frache, S. Coluccia, L. Marchese, in preparation.
[37] M. Stöcker, Micropor. Mesopor. Mater. 29 (1999) 3.
[38] L. Marchese, A. Frache, G. Gatti, S. Coluccia, L. Lisi, G. Ruoppolo, G. Russo, H.O. Pastore, J. Catal. 208 (2002) 479.
[39] J. Chen, P.A. Wright, J.M. Thomas, S. Natarajan, L. Marchese, S.M. Bradley, G. Sankar, C.R.A. Catlow, P.L. Gai-Boyes, R.P. Towsend, C.M. Lok, J. Phys. Chem. 98 (1994) 10216.
[40] L. Marchese, J. Chen, P.A. Wright, J.M. Thomas, J. Phys. Chem. 97 (1993) 8109.
[41] E.M. Flanigen, R.L. Patton, S.T. Wilson, Stud. Surf. Sci. Catal. 37 (1988) 13.
[42] M.T. Melchior, J.M. Newsam, Stud. Surf. Sci. Catal. 49 (1989) 805.
[43] S. Coluccia, E. Gianotti, L. Marchese, Mater. Sci. Eng. C 15 (2002) 219.
[44] J.M. Thomas, G.N. Greaves, G. Sankar, P.A. Wright, J. Chen, A.J. Dent, L. Marchese, Angew. Chem. Int. Ed. Engl. 33 (1994) 1871.
[45] M.P.J. Peeters, J.H.C. van Hoof, R.A. Sheldon, V.L. Zholobenko, L.M. Kustov, V.B. Kazansky, in: R. von Ballmoos, J.B. Higgins, M.M.J. Treacy (Eds.), Proceedings of the Ninth IZC, vol. I, Butterworths/Heinemann, Washington, DC, 1993, p. 651.
[46] R. De Vos, J. Pelgrims, H. Leeman, Stud. Surf. Sci. Catal. 49 (1989) 559.
[47] E. Gianotti, M.C. Paganini, G. Martra, E. Giamello, S. Coluccia, L. Marchese, Stud. Surf. Sci. Catal. 135 (2001) 178.
[48] E. Gianotti, L. Marchese, G. Martra, S. Coluccia, Catal. Today 54 (1999) 547.
[49] R.I. Soltanov, Kinet. Katal. 31 (1990) 438.
[50] A.W. Aylor, L.J. Lobree, J.A. Reimer, A.T. Bell, Stud. Surf. Sci. Catal. 101 (1996) 661.
[51] R. Pirone, P. Ciambelli, G. Moretti, G. Russo, Appl. Catal. B 8 (1996) 197.
[52] P. Ciambelli, Private communication.
[53] G. Spoto, A. Zecchina, S. Bordiga, G. Ricchiardi, G. Martra, G. Leofanti, G. Petrini, Appl. Catal. B 3 (1994) 151.
[54] A. Zecchina, D. Scarano, G. Spoto, S. Bordiga, C. Lamberti, G. Bellussi, Stud. Surf. Sci. Catal. 117 (1998) 343.
[55] Y. Kuroda, R. Kumashiro, T. Yoshimoto, M. Nagao, Chem. Phys. 1 (1999) 649.
[56] J. Dedecek, B. Wichterlová, P. Kubát, Micropor. Mesopor. Mater. 32 (1999) 63.
[57] M.V. Konduru, S.S.C. Chuang, J. Phys. Chem. B 103 (1999) 5802.
[58] P. Ciambelli, G. Moretti, G. Russo, Catal. Lett. 43 (1997) 255.
[59] P. Ciambelli, A. Di Benedetto, E. Garufi, R. Pirone, G. Russo, J. Catal. 175 (1998) 161.